AGU ADVANCING EARTH AND SPACE SCIENCE

Geophysical Research Letters®

RESEARCH LETTER

10.1029/2021GL095389

Key Points:

- Electric field measurements in Antarctica show that strong El Niños and La Niñas consistently impact the atmospheric global circuit
- For the super El Niño event of 2015/16, the anomalies in the global electric circuit are especially pronounced
- Simulations show that the observed effect is due to changes in deep convection over the Pacific Ocean, Maritime Continent, and South America

Supporting Information:

Supporting Information may be found in the online version of this article.

Correspondence to:

N. N. Slyunyaev,
slyunyaev.n@ipfran.ru

Citation:

Slyunyaev, N. N., Frank-Kamenetsky, A. V., Ilin, N. V., Sarafanov, F. G., Shatalina, M. V., Mareev, E. A., & Price, C. G. (2021). Electric field measurements in the Antarctic reveal patterns related to the El Niño—Southern Oscillation. *Geophysical Research Letters*, *48*, e2021GL095389. https://doi.org/10.1029/2021GL095389

Received 22 JUL 2021
Accepted 19 OCT 2021

Author Contributions:

Conceptualization: Nikolay N. Slyunyaev, Nikolay V. Ilin, Evgeny A. Mareev, Colin G. Price
Data curation: Alexander V. Frank-Kamenetsky
Formal analysis: Nikolay N. Slyunyaev
Investigation: Alexander V. Frank-Kamenetsky
Methodology: Nikolay N. Slyunyaev, Alexander V. Frank-Kamenetsky, Nikolay V. Ilin, Evgeny A. Mareev
Software: Nikolay V. Ilin, Fedor G. Sarafanov, Maria V. Shatalina
Supervision: Evgeny A. Mareev, Colin G. Price
Visualization: Nikolay N. Slyunyaev

Electric Field Measurements in the Antarctic Reveal Patterns Related to the El Niño—Southern Oscillation

Nikolay N. Slyunyaev[1], Alexander V. Frank-Kamenetsky[2], Nikolay V. Ilin[1], Fedor G. Sarafanov[1,3], Maria V. Shatalina[1], Evgeny A. Mareev[1,3], and Colin G. Price[1,4]

[1]Institute of Applied Physics, Russian Academy of Sciences, Nizhny Novgorod, Russia, [2]Arctic and Antarctic Research Institute, St. Petersburg, Russia, [3]Department of Radiophysics, Lobachevsky State University of Nizhny Novgorod, Nizhny Novgorod, Russia, [4]Department of Geophysics, Tel Aviv University, Tel Aviv, Israel

Abstract Electric field measurements at Vostok station in Antarctica reveal that the El Niño—Southern Oscillation (ENSO) has a statistically significant effect on the global electric circuit, as earlier predicted by simulations. Analysis of 10 October-February periods during 2006–2016 indicates that the shape of the diurnal variation of the surface electric field is significantly different for El Niño and La Niña years, with an especially pronounced deviation during the super El Niño of 2015/16. During strong El Niños the potential gradient relative to the diurnal mean is generally higher than usual around 8:00–14:00 UTC and lower than usual around 16:00–0:00 UTC; La Niñas are characterized by the opposite behavior. Simulations with the Weather Research and Forecasting model imply that the observed patterns are the result of changes in the global distribution of electrified clouds over the Pacific Ocean, Maritime Continent, and South America during ENSO events.

Plain Language Summary The El Niño—Southern Oscillation (ENSO) is one of the most remarkable modes of climate variability on Earth. Being made up of irregularly alternating warm (El Niño) and cold (La Niña) phases, the ENSO affects atmospheric circulation, global temperature and rainfall patterns, agriculture, and economic output. Recent simulations have suggested that changes in global convection patterns due to ENSO should also affect surface atmospheric electric fields and currents in remote regions of the planet. Here, we present electric field measurements performed during 2006–2016 at Vostok station in the Antarctic that reveal clear patterns related to ENSO as earlier predicted by simulations. Measurements show that the shape of the diurnal variation of the surface electric field is significantly different for El Niño and La Niña years (with an especially pronounced effect during the super El Niño of 2015/16), which, according to simulations, is the result of changes in the global distribution of electrified clouds over the Pacific Ocean, Maritime Continent, and South America during ENSO events. This provides further evidence of the influence of climate fluctuations on the Earth's global electromagnetic environment.

1. Introduction

The El Niño—Southern Oscillation (ENSO) is one of the most conspicuous modes of climate variability (e.g., McPhaden et al., 2020). After the seasonal cycle of summer and winter, the ENSO is the largest cause of climate variations on Earth. The ENSO cycle is made up of warm (El Niño) and cold (La Niña) phases, which replace each other at irregular intervals. During El Niños and La Niñas, the central and eastern equatorial Pacific Ocean heats or cools by a few degrees for 12–18 months, which has major impacts on global temperature (Tsonis et al., 2005) and rainfall (Villafuerte & Matsumoto, 2015) patterns, agriculture and economic output (Adams et al., 1999), and even public health (Kovats et al., 2003).

ENSO events are characterized by notable shifts in atmospheric convection patterns, affecting both the north-south Hadley circulation and the east-west Walker circulation. Considering that tropical deep convection is associated with thunderstorms and lightning, it should not be surprising that the ENSO also influences the Earth's electrical environment. However, while the effect of ENSO on lightning has been widely discussed in the literature (Chronis et al., 2008; Goodman et al., 2000; Hamid et al., 2001; Kumar & Kamra, 2012; Price, 2009; Price & Federmesser, 2006; Sátori & Zieger, 1999; Sátori et al., 2009; Williams, 1992;

Writing – original draft: Nikolay N. Slyunyaev
Writing – review & editing: Alexander V. Frank-Kamenetsky, Nikolay V. Ilin, Fedor G. Sarafanov, Maria V. Shatalina, Evgeny A. Mareev, Colin G. Price

Williams et al., 2021; Yoshida et al., 2007), little attention has been given to its influence on quasi-stationary electric fields and currents in the atmosphere.

Such fields and currents form the so-called global electric circuit (GEC; see Rycroft et al., 2000; Tinsley, 2008; Williams, 2009; Williams & Mareev, 2014), which is arguably the most overarching concept in atmospheric electricity. The idea of the GEC is based on Wilson's (1921, 1924) hypothesis, which suggests that charge separation inside thunderstorms and electrified shower clouds drives the quasi-stationary current upward (toward the ionosphere), whereas in fair-weather regions this current eventually returns to the Earth's surface, with the highly conducting Earth and ionosphere completing the electrical network.

The electric potential of the ionosphere relative to the Earth's surface, maintained by thunderstorms and electrified shower clouds all over the Earth and referred to as the ionospheric potential (IP), is the most natural characteristic of the GEC intensity (see, e.g., Markson, 1986). However, there have been only few studies aimed at measuring the IP directly, since such measurements require expensive aircraft flights or balloon soundings (Markson, 2007). On the other hand, it has long been known that the fair-weather potential gradient (PG), when shown as a function of universal time, looks nearly the same at different locations (Mauchly, 1921, 1923) and reflects the diurnal cycle of global thunderstorm activity (Whipple & Scrase, 1936). This implies that even the results of surface PG measurements at a single location (which, unlike IP measurements, can be performed on a regular basis) should contain some information about the global structure of convection.

Recent attempts to simulate the IP variation by modeling the atmospheric dynamics have suggested that changes in global convection patterns due to ENSO should indeed notably affect the GEC intensity and shape of its diurnal variation (Slyunyaev et al., 2021a, 2021b). However, until now there have been only few studies searching for the impact of ENSO in the results of atmospheric electricity measurements. Harrison et al. (2011) analyzed the results of PG measurements performed at the Shetland Islands during 1968–1984 and reported a positive correlation between the ENSO cycle and the mean fair-weather PG in December, with a maximum sensitivity of PG values to the ENSO around 12:00 UTC. More recently, Lavigne et al. (2017) employed the results of PG measurements at Vostok station in Antarctica in 1998–2004 and 2007–2011 to show that El Niño and La Niña years are characterized by different patterns of the PG variation, noting in particular an enhancement of the PG at 16:00–0:00 UTC in January-April in La Niña years.

Here, we shall also focus on the diurnal variation of the GEC, which contains more information about convection than the mean GEC intensity. We shall analyze the results of PG measurements at Vostok performed during 2006–2016 (part of these data were earlier used by Lavigne et al., 2017). In contrast to previous studies of the relationship between the GEC and ENSO, we shall look only at the shape of the diurnal variation of the PG, thus excluding the year-to-year variability of the mean, which is to a large extent related to the local variation of conductivity (e.g., due to the solar cycle). This will enable us to show that the results of PG measurements in the Antarctic indeed contain clearly visible patterns related to ENSO, with a statistically significant difference between the PG behavior in El Niño and La Niña years. Then simulations with the Weather Research and Forecasting (WRF) model on the basis of meteorological reanalysis data will help us to account for the mechanism behind this effect.

2. Methods

2.1. Atmospheric Electricity Measurements at Vostok Station

We use the results of continual PG measurements at the Russian Vostok station in the Antarctic (78.5°S, 106.9°E, 3,488 m above sea level) during 2006–2016. While midlatitude surface PG measurements at land sites are usually affected by local factors such as aerosols or natural radioactivity, measurements in clean locations on the high Antarctic plateaux offer a unique opportunity to identify even subtle trends in the GEC variability (Burns et al., 2012, 2017).

The rotating-dipole field mill for measuring the atmospheric PG, which presently operates at Vostok station, has been installed at the very end of 2005 under an agreement between the Russian Antarctic Expedition and the Australian Antarctic Division (Burns et al., 2017). The field mill is placed on a metal pole about 3 m above the snow surface, upwind of the main station buildings; the rotational speed of the dipole is about 1,600 revolutions per minute. Note that the field mill that operated at Vostok in 1998–2004 (Burns et al., 2005, 2012) was different from the present one.

The results of PG measurements are collected in the form of mean values over consecutive 10-s periods. Since the metal pole supporting the field mill clearly disturbs recorded electric field values, collected PG values must be divided by a certain form factor to obtain the actual ones. Simultaneous PG measurements involving two identical field mills, one of which was placed on the aforementioned 3-m pole with a long thin wire at a high voltage stretched above it, have shown that this form factor is nearly equal to 3. A division by this value has been applied to the results of PG measurements at Vostok throughout this study. A high accuracy in determining the form factor is not important to us here, for in this particular study we always look at PG values relative to the diurnal mean.

2.2. Processing of the PG Data

It is known that sea surface temperature (SST) anomalies in the Pacific associated with ENSO events are most pronounced during Northern Hemisphere winters. Therefore, here, we focus our attention on 5-month periods around Decembers of different years (October-February). For the 10 such periods in 2006–2016, we use the whole data set of available PG measurements. To simplify further analysis, we transformed the 10-s data collected by the field mill into average values over consecutive UTC hours. Sometimes there are small gaps in the data; for this reason, when averaging, we retained only those hours for which at least 80% of the 10-s PG values are known.

When analyzing the results of PG measurements, it is important to exclude the data affected by bad weather conditions before taking an average over a large number of days. When dealing with PG measurements in the Antarctic, one does not necessarily need to use meteorological data in order to identify fair-weather days, and criteria based on PG values alone usually work well (Burns et al., 2005, 2012, 2017). Therefore, to select fair-weather days for this study, we applied the following formal procedure:

1. The days with incomplete/absent hourly data have been excluded
2. The days with negative/zero hourly PG values have been excluded
3. The days with hourly PG values exceeding 300 V/m have been excluded
4. Among the remaining days only those have been retained for which the diurnal peak-to-peak amplitude does not exceed 150% of the diurnal mean

When computing the average diurnal variation of the PG at Vostok for each individual October-February period during 2006–2016, we use only the data for fair-weather days within this period, identified by means of the procedure described above.

2.3. Simulation of the GEC With the WRF Model

Surface PG measurements in clean locations are generally able to reproduce the main trends in the variation of the GEC intensity; at the same time, the results of such measurements do not give us any information about the origin of these trends. In order to shed further light on the results of measurements, it is useful to recall that the GEC is maintained by global electrified clouds, which implies that its variation can also be simulated on the basis of modeling the atmospheric dynamics (Mareev & Volodin, 2014). More precisely, grid cell contributions to the IP can be parameterized in terms of convection and precipitation (Ilin et al., 2020; Slyunyaev et al., 2019), which makes it possible not only to determine the total IP (perhaps the most fundamental measure of the GEC intensity) but also to decompose it as a sum of regional constituents, which may reveal the mechanisms behind the variation of the GEC (Slyunyaev et al., 2021b).

Although such simulations with weather and climate models are known to generally underestimate the peak-to-peak amplitude of the diurnal variation of GEC parameters, they yield satisfactory results during Northern Hemisphere winters (see Ilin et al., 2020), which are most important for the ENSO. For this study, we calculated the total IP and regional contributions to it for the same October-February periods of 2006–2016, using the WRF model (Powers et al., 2017; Skamarock et al., 2019) and meteorological reanalysis data for the simulation of the atmospheric dynamics.

More precisely, we ran the WRF globally on a 1° × 1° latitude-longitude grid (see Supporting Information S1 for other technical details) to simulate the atmospheric dynamics on every third day, which is enough to obtain a stable diurnal variation curve for each October-February season. To initialize the WRF for each model run, we used the ERA5 data on pressure levels (Hersbach et al., 2018). ERA5 stands for the fifth generation ECMWF (European Centre for Medium-Range Weather Forecasts) reanalysis for the global climate and weather; it combines model data with global observations into a consistent data set.

To calculate the IP and regional contributions to it, we used the parameterization suggested by Slyunyaev et al. (2019) on the basis of an earlier idea of Mareev and Volodin (2014); a detailed discussion of this parameterization can be found in Ilin et al. (2020). The formula expressing the IP in terms of climate variables is included in Supporting Information S1 for this article, while here we just mention that the two most important features of this parameterization are (i) cutting off the grid columns with weak convective activity on the basis of convective available potential energy and (ii) estimating the area covered by electrified clouds (i.e., the generators of the GEC) in each column from the amount of precipitation. Note that such a parameterization is supposed to take into account both thunderstorms and electrified shower clouds.

Finally, the diurnal variation of the IP for each individual October-February period is obtained by averaging over a large number of days and employing some regularization procedures, described in Supporting Information S1.

3. Results

3.1. Effect of ENSO on the Diurnal Variation of Atmospheric Electricity

It is not so easy to observe the effect of individual ENSO events in the results of surface PG measurements, as even in the Antarctic such measurements are influenced by variable local factors so that one needs a large number of fair-weather days to obtain a stable curve of the average diurnal variation. Therefore, we first look at the data for all El Niño or La Niña years *combined together*, using SST anomalies in the so-called Niño 3.4 region (5°S–5°N, 120°–170°W) to determine the phase of the ENSO cycle. Such anomalies, computed relative to long-term averages taken over several decades, provide one of the most widely used indices characterizing the ENSO: large positive and negative anomalies indicate El Niño and La Niña events, respectively. In this study, we use 5-month Niño 3.4 SST anomalies, calculated relative to the 30-year mean on the basis of a monthly time series of Niño 3.4 SST values by National Oceanic and Atmospheric Administration (NOAA) Climate Prediction Center (CPC); further details are given in Supporting Information S1.

More precisely, we divide all winter seasons that we consider (2006/07 to 2015/16) into two groups based on the sign of the 5-month Niño 3.4 SST anomaly. Figure 1a shows the diurnal variations of the PG for October-February, when averaged over each of these two groups (with the year-to-year variability of the 5-month mean removed; see Supporting Information S1 for more details). We observe a systematic change in the diurnal variation with the ENSO cycle: The PG relative to the diurnal mean around 10:00 UTC is higher in El Niño years and lower in La Niña years, whereas around 18:00 UTC it behaves oppositely.

If we consider only strong El Niño and La Niña events (say, those with the 5-month Niño 3.4 SST anomaly of +0.9 °C or greater or of −0.9 °C or smaller), we see a much more pronounced effect. This is shown in Figure 1b, where the diurnal variation of the PG at Vostok during two strong El Niños that occurred during 2006–2016 (2009/10, 2015/16) is compared with its counterpart for three strong La Niñas in the same time span (2007/08, 2010/11, 2011/12). A positive response of the relative PG to ENSO during 8:00–14:00 UTC and a negative response during 16:00–0:00 UTC are clearly seen. These results are generally consistent with earlier observations by Harrison et al. (2011), who have reported that the PG is most sensitive to the ENSO around 12:00 UTC, and by Lavigne et al. (2017), who have established an increase in the PG at 16:00–0:00 UTC in La Niña years. However, one should be careful when making such comparisons, as here we do not consider absolute PG values at all.

Figures 1c and 1d show the simulated diurnal variations of the IP corresponding to Figures 1a and 1b, respectively. We see the same effect as that observed in measurements: A positive response of the relative IP to ENSO around 8:00–14:00 UTC and a negative response around 16:00–0:00 UTC, which agrees with earlier simulations (Slyunyaev et al., 2021a). As before, in the case of strong events, the effect is more pronounced.

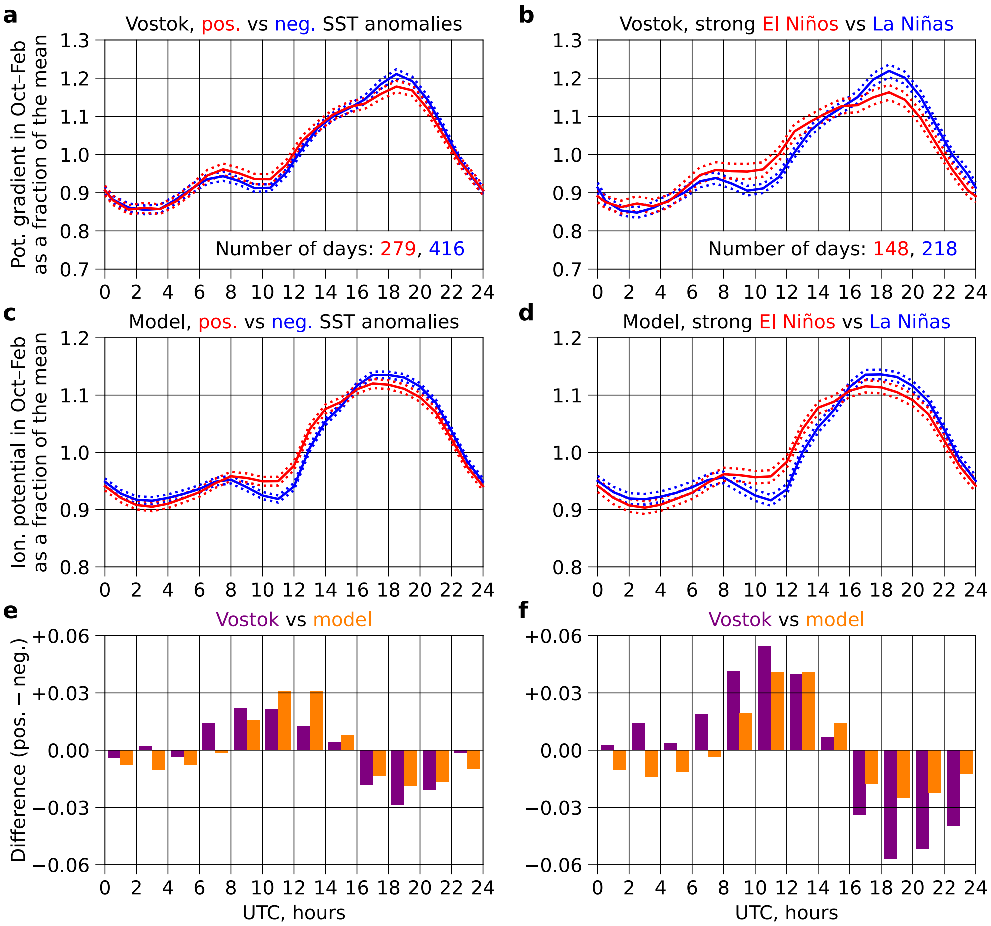

Figure 1. (a) The diurnal variation of the potential gradient (PG) at Vostok in October-February for the years characterized by positive (red curve) and negative (blue curve) Niño 3.4 sea surface temperature (SST) anomalies (with the year-to-year variability removed). Dotted lines show diurnal variations plus and minus one standard error. (b) Similar to (a) for the years with strong El Niños and La Niñas (those with the 5-month Niño 3.4 SST anomaly of ±0.9 °C or larger). (c), (d) Similar to (a) and (b) for the ionospheric potential (IP) simulated using the Weather Research and Forecasting (WRF) model. (e) Two-hour mean values of the difference between the two curves shown in (a) and (b). (f) Similar to (e) for (b) and (d).

Figures 1e and 1f quantify the similarity between the results of measurements and the results of modeling, demonstrating that 2-h differences between the relative PG values and 2-h differences between the relative IP values behave similarly (a time shift of about 1–2 h between the variations of measured and modeled differences during 6:00–16:00 UTC is apparently related to shortcomings of simulations, which are inevitable on large-scale grids, where microphysical characteristics of clouds are not available and one cannot faithfully separate electrified clouds from nonelectrified ones; see Ilin et al., 2020).

Next, we will look at the results of PG measurements for *individual* years. Being based on a smaller number of days, diurnal variation curves for individual October-February seasons are less reliable than long-term ones, but it is still interesting to compare their shapes in El Niño and La Niña years. In Figures 2a–2d, we show diurnal variation curves of the PG for four individual October-February periods together with the average diurnal variation plotted on the basis of all October-February periods during 2006–2016 (with the year-to-year variability of the 5-month mean eliminated). For these four periods, each of which was accompanied by a large Niño 3.4 SST anomaly, we indeed observe in the results of PG measurements certain patterns related to ENSO: During strong El Niños, the relative GEC intensity is higher than usual around 8:00–14:00 UTC and lower than usual around 18:00–0:00 UTC; strong La Niñas are characterized by the opposite behavior. The results of IP simulation, shown in Figures 2e–2h, demonstrate the same effect in a clearer manner.

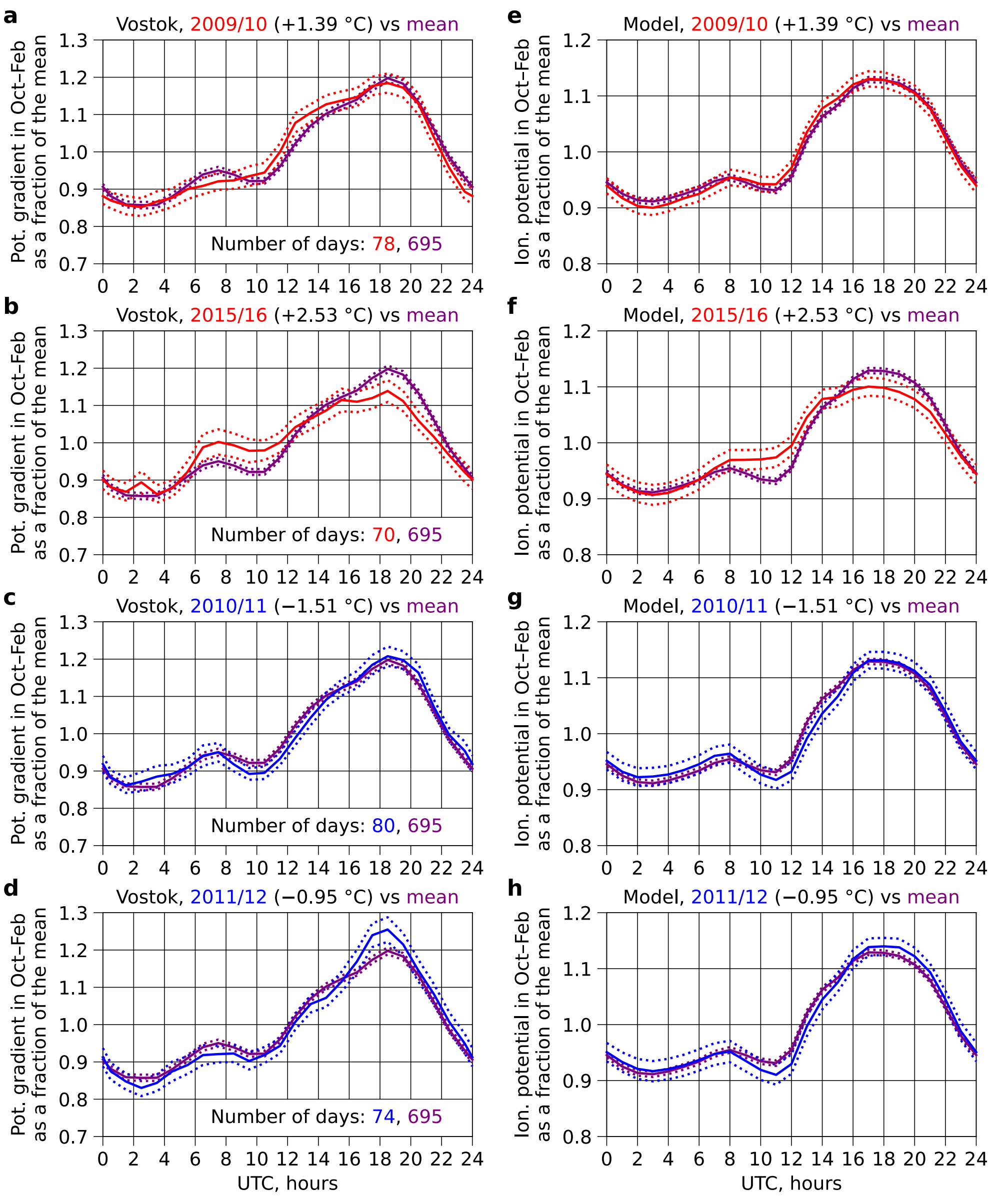

Figure 2. (a)–(d) The diurnal variation of the potential gradient (PG) at Vostok in October-February for certain individual years characterized by pronounced El Niño or La Niña events (red and blue curves) and on average with the year-to-year variability removed (purple curve). Dotted lines show diurnal variations plus and minus one standard error; temperatures in parentheses indicate the 5-month Niño 3.4 sea surface temperature (SST) anomalies. Similar plots for other years are given in Figure S1 in Supporting Information S1. (e)–(h) Similar to (a)–(d) for the IP simulated using the Weather Research and Forecasting (WRF) model.

However, even these results for individual El Niño and La Niña years do not appear as clear as the long-term averages shown in Figure 1. For other years with considerably high Niño 3.4 SST anomalies (including the strong La Niña event of 2007/08) the ENSO-driven patterns are not always distinctly seen either (see Figure S1 in Supporting Information S1), which can apparently be attributed to PG fluctuations due to local effects. In this connection, the super El Niño event of 2015/16 is especially interesting, as for this event both measurements (Figure 2b) and modeling (Figure 2f) show a very pronounced deviation of the diurnal variation curve from the long-term mean.

Dotted lines in Figures 1 and 2 show one standard error bands around each curve (see Supporting Information S1 for more details on calculating standard errors in this study). When we compare strong El Niños

10.1029/2021GL095389

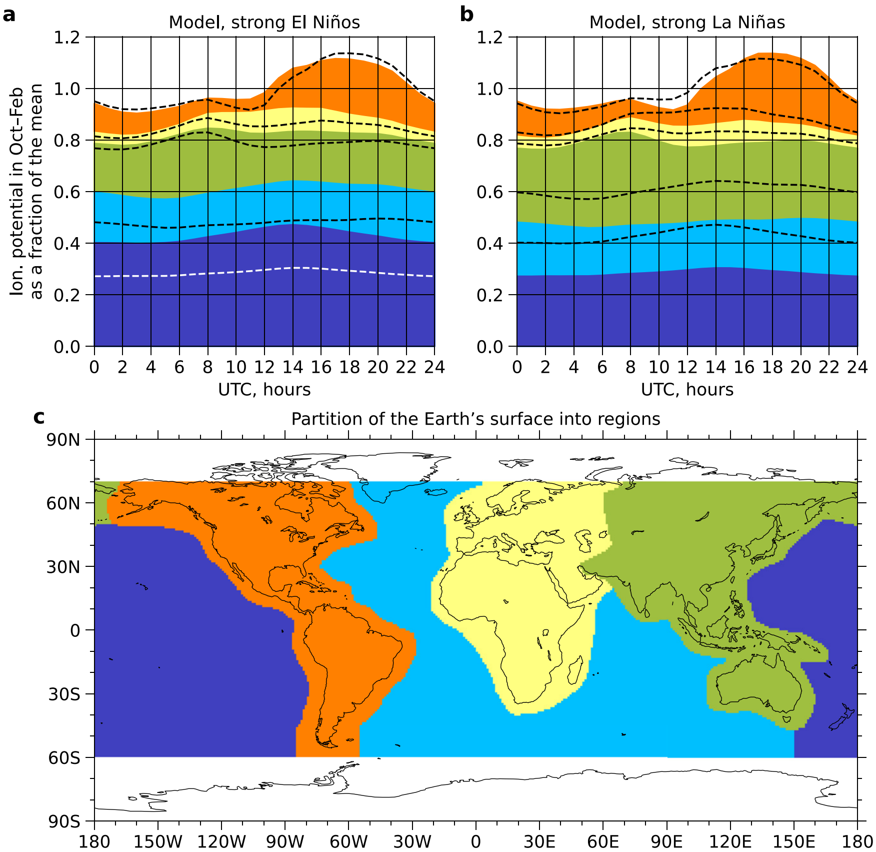

Figure 3. (a) The diurnal variation of the ionospheric potential (IP) in October-February during strong El Niños simulated using the Weather Research and Forecasting (WRF) model (the red curve of Figure 1d), shown cumulatively as the sum of contributions from different regions of the Earth's surface. (b) Similar to (a) for strong La Niñas (the blue curve of Figure 1d). In each of these two panels dashed lines demonstrate contributions shown in the other one. A similar comparison for individual regions is given in Figure S2 in Supporting Information S1. (c) The partition of the Earth's surface into regions used in (a) and (b): Pacific Ocean, Atlantic Ocean and Indian Ocean, Asia and Australia, Europe and Africa, Americas. The contribution of polar regions (white) is negligibly small.

with strong La Niñas (Figure 1b) and when we compare the super El Niño season of 2015/16 with the long-term mean (Figure 2b), we observe that the discovered effect is, in a certain sense, statistically significant.

3.2. Explanation of the Mechanism Behind the Observed Effect

Simulation of the IP makes it possible to explain the formation of the patterns observed in the diurnal variation curve. In Figure 3, the diurnal variations of Figure 1d are shown cumulatively as sums of contributions from five global regions of the Earth's surface. Systematic changes in equatorial convection in El Niño and La Niña years make regional contributions to the GEC increase and decrease, thereby changing the shape of its diurnal variation.

It appears that the relative contribution of Atlantic and Indian Oceans and the contribution of Europe and Africa do not change much with ENSO. The contribution of the Pacific Ocean is positively correlated with the ENSO cycle, while the contributions of Asia and Australia (to a large extent determined by the Maritime Continent) and the Americas (mostly South America in October-February periods, which we consider) show a negative correlation (cf. Slyunyaev et al., 2021b).

It is known that contributions of land regions to the GEC reach their diurnal maxima around 16:00 local time (Mach et al., 2011; Slyunyaev et al., 2019), while contributions of oceans are much flatter, with less pronounced maxima around 4:00 local time (Slyunyaev et al., 2019). It is therefore not surprising that the change due to ENSO in the Americas' contribution is especially pronounced at around 14:00–0:00 UTC,

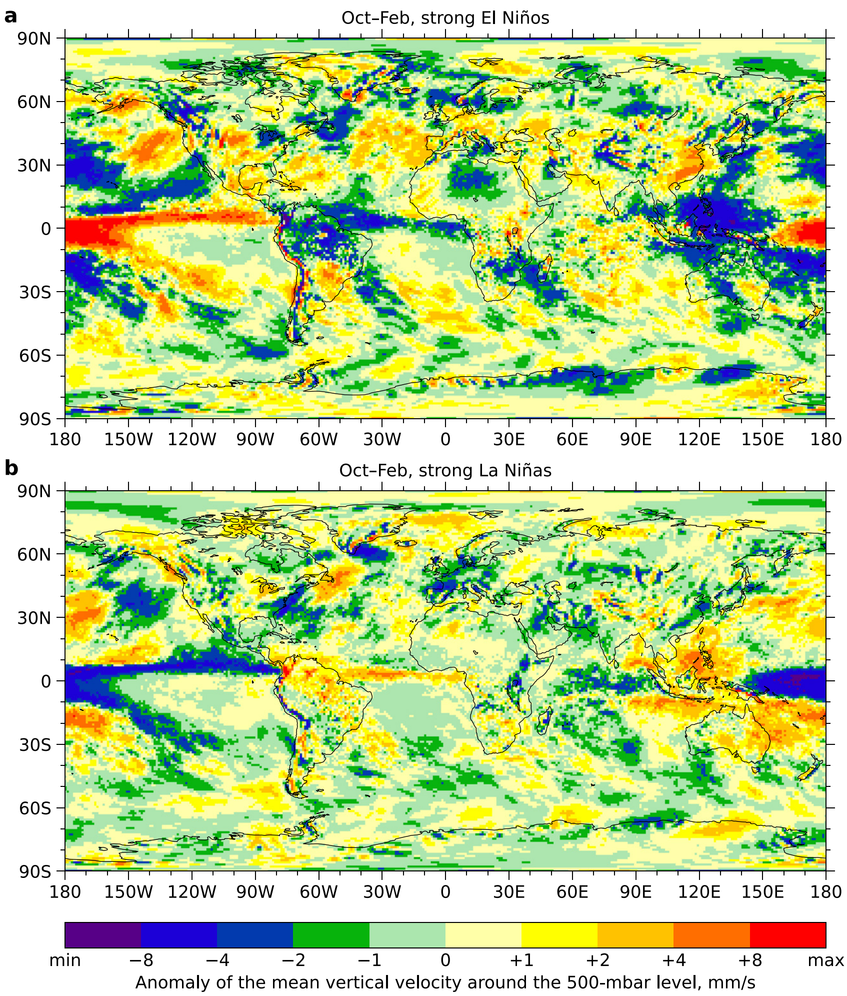

Figure 4. (a) Anomalies of the simulated mean vertical velocity in October-February at the Weather Research and Forecasting (WRF) level around 500 mbar during strong El Niños. (b) Similar to (a) for strong La Niñas.

while the change in the contribution of the Pacific Ocean is greater than usual at around 8:00–20:00 UTC (i.e., changes in contributions are most prominent near the maxima of these contributions; see Figure S2 in Supporting Information S1 where the regional contributions are plotted separately). On the other hand, the contribution from Asia and Australia changes with ENSO more or less uniformly; this may be a consequence of the fact that in our partition of the Earth's surface this region is a mixture of land and ocean, so that one should not expect it to have a single pronounced maximum.

In view of all this, we conclude that the negative response to ENSO of the Americas' contribution accounts for the negative response of the diurnal variation curve at 16:00–0:00 UTC, as observed in Figures 1 and 2. At the same time, the positive effect observed at 8:00–14:00 UTC can be attributed to a positive response of the Pacific Ocean (or, more precisely, to its part that is not compensated by a negative response from Asia and Australia).

Figure 4 further illustrates this mechanism, showing the geographical distribution of anomalies in the simulated mean vertical velocity at the WRF level around 500 mbar during strong El Niño and La Niña events. These anomalies are computed for each model pixel as the difference between the velocity averaged over the seasons accompanied by strong El Niños or La Niñas and the long-term mean over all October-February seasons in 2006–2016. The positive response to the ENSO of convection over the Pacific Ocean and the negative response of that over the Maritime Continent and South America are clearly seen.

4. Conclusions

The results of this study clearly indicate that changes in global convection patterns have an influence on global atmospheric electricity, making the effect of ENSO detectable even in the results of electric field measurements in Antarctica, far from the equatorial regions affected by El Niño and La Niña events directly. Although fluctuations due to local effects do not allow one to distinctly see ENSO-related patterns for each individual year, for the majority of strong events they are clearly seen (and the effect is statistically significant, provided that we take the average over a sufficiently large number of days). During strong El Niños the relative PG at Vostok is generally higher than usual around 8:00–14:00 UTC and lower than usual around 16:00–0:00 UTC, whereas La Niñas are characterized by the opposite behavior. It is worthy of note that this effect is especially pronounced in the case of the 2015/16 super El Niño event.

It is important that simulations with the WRF support the results of PG measurements at Vostok, predicting the same effect of the ENSO on the diurnal variation of the GEC. What is even more important, theoretical modeling is able to reveal the mechanism behind the observed relationship. According to simulations, convection over the Pacific Ocean intensifies during strong El Niños and lessens during strong La Niñas, while convection over the Maritime Continent and South America behaves oppositely. This makes contributions of these regions to the GEC higher or lower during ENSO events, which eventually results in the observed changes in the shape of the diurnal variation of the GEC.

Data Availability Statement

Hourly PG data from Vostok, source codes and scripts used to analyze the results and plot the images are available at https://eee.ipfran.ru/files/enso-gec-2021/grl. The WRF model can be downloaded from https://www2.mmm.ucar.edu/wrf/users. Simulations with the WRF model used the ERA5 data (Hersbach et al., 2018), downloaded from the Copernicus Climate Change Service (C3S) Climate Data Store, so that their results contain modified C3S information 2021; neither the European Commission nor ECMWF is responsible for any use that may be made of the Copernicus information or data it contains. A time series of monthly Niño 3.4 SST values by NOAA CPC, which was used to compute Niño 3.4 SST anomalies, is available online at https://psl.noaa.gov/data/correlation/nina34.data.

Acknowledgments

This work was supported by a grant from the Government of the Russian Federation (contract no. 075-15-2019-1892). The authors are grateful to the Australian Antarctic Division, namely to Gary Burns, the chief investigator of the project "Atmospheric electrical circuits, weather and climate research," and to Lloyd Simons for their contribution to the development of instruments and software for collecting the electric field data at Vostok station. Continuous registration and collection of the electric field data at Vostok station is carried out by the specialists of the Russian Antarctic Expedition within the framework of the project "Integrated oceanological, climatic, glaciological, and geophysical studies of Antarctica and the Southern Ocean."

References

Adams, R. M., Chen, C.-C., McCarl, B. A., & Weiher, R. F. (1999). The economic consequences of ENSO events for agriculture. *Climate Research*, *13*(3), 165–172. https://doi.org/10.3354/cr013165

Burns, G. B., Frank-Kamenetsky, A. V., Tinsley, B. A., French, W. J., Grigioni, P., Camporeale, G., & Bering, E. A. (2017). Atmospheric global circuit variations from Vostok and Concordia electric field measurements. *Journal of the Atmospheric Sciences*, *74*(3), 783–800. https://doi.org/10.1175/JAS-D-16-0159.1

Burns, G. B., Frank-Kamenetsky, A. V., Troshichev, O. A., Bering, E. A., & Reddell, B. D. (2005). Interannual consistency of bi-monthly differences in diurnal variations of the ground-level, vertical electric field. *Journal of Geophysical Research*, *110*, D10106. https://doi.org/10.1029/2004JD005469

Burns, G. B., Tinsley, B. A., Frank-Kamenetsky, A. V., Troshichev, O. A., French, W. J. R., & Klekociuk, A. R. (2012). Monthly diurnal global atmospheric circuit estimates derived from Vostok electric field measurements adjusted for local meteorological and solar wind influences. *Journal of the Atmospheric Sciences*, *69*(6), 2061–2082. https://doi.org/10.1175/JAS-D-11-0212.1

Chronis, T. G., Goodman, S. J., Cecil, D., Buechler, D., Robertson, F. J., Pittman, J., & Blakeslee, R. J. (2008). Global lightning activity from the ENSO perspective. *Geophysical Research Letters*, *35*, L19804. https://doi.org/10.1029/2008GL034321

Goodman, S. J., Buechler, D. E., Knupp, K., Driscoll, K., & McCaul, E. W., Jr. (2000). The 1997–98 El Nino event and related wintertime lightning variations in the southeastern United States. *Geophysical Research Letters*, *27*(4), 541–544. https://doi.org/10.1029/1999GL010808

Hamid, E. Y., Kawasaki, Z., & Mardiana, R. (2001). Impact of the 1997–98 El Niño Event on lightning activity over Indonesia. *Geophysical Research Letters*, *28*(1), 147–150. https://doi.org/10.1029/2000GL011374

Harrison, R. G., Joshi, M., & Pascoe, K. (2011). Inferring convective responses to El Niño with atmospheric electricity measurements at Shetland. *Environmental Research Letters*, *6*(4), 044028. https://doi.org/10.1088/1748-9326/6/4/044028

Hersbach, H., Bell, B., Berrisford, P., Biavati, G., Horányi, A., Muñoz Sabater, J., et al. (2018). *ERA5 hourly data on pressure levels from 1979 to present*. Copernicus Climate Change Service (C3S) Climate Data Store (CDS). https://doi.org/10.24381/cds.bd0915c6

Ilin, N. V., Slyunyaev, N. N., & Mareev, E. A. (2020). Toward a realistic representation of global electric circuit generators in models of atmospheric dynamics. *Journal of Geophysical Research: Atmospheres*, *125*, e2019JD032130. https://doi.org/10.1029/2019JD032130

Kovats, R. S., Bouma, M. J., Hajat, S., Worrall, E., & Haines, A. (2003). El Niño and health. *The Lancet*, *362*(9394), 1481–1489. https://doi.org/10.1016/S0140-6736(03)14695-8

Kumar, P. R., & Kamra, A. K. (2012). Variability of lightning activity in South/Southeast Asia during 1997–98 and 2002–03 El Nino/La Nina events. *Atmospheric Research*, *118*, 84–102. https://doi.org/10.1016/j.atmosres.2012.06.004

Lavigne, T., Liu, C., Deierling, W., & Mach, D. (2017). Relationship between the global electric circuit and electrified cloud parameters at diurnal, seasonal, and interannual timescales. *Journal of Geophysical Research: Atmospheres*, *122*, 8525–8542. https://doi.org/10.1002/2016JD026442

Mach, D. M., Blakeslee, R. J., & Bateman, M. G. (2011). Global electric circuit implications of combined aircraft storm electric current measurements and satellite-based diurnal lightning statistics. *Journal of Geophysical Research*, *116*, D05201. https://doi.org/10.1029/2010JD014462

Mareev, E. A., & Volodin, E. M. (2014). Variation of the global electric circuit and ionospheric potential in a general circulation model. *Geophysical Research Letters*, *41*, 9009–9016. https://doi.org/10.1002/2014GL062352

Markson, R. (1986). Tropical convection, ionospheric potentials and global circuit variation. *Nature*, *320*(6063), 588–594. https://doi.org/10.1038/320588a0

Markson, R. (2007). The global circuit intensity: Its measurement and variation over the last 50 years. *Bulletin of the American Meteorological Society*, *88*(2), 223–242. https://doi.org/10.1175/BAMS-88-2-223

Mauchly, S. J. (1921). Note on the diurnal variation of the atmospheric-electric potential-gradient. *Physical Review*, *18*(2), 161–162. https://doi.org/10.1103/PhysRev.18.85

Mauchly, S. J. (1923). On the diurnal variation of the potential gradient of atmospheric electricity. *Terrestrial Magnetism and Atmospheric Electricity*, *28*(3), 61–81. https://doi.org/10.1029/TE028i003p00061

McPhaden, M. J., Santoso, A., & Cai, W. (Eds.), (2020). *El Niño Southern Oscillation in a changing climate* (Geophysical Monograph Series 253). John Wiley & Sons, Inc.—American Geophysical Union. https://doi.org/10.1002/9781119548164

Powers, J. G., Klemp, J. B., Skamarock, W. C., Davis, C. A., Dudhia, J., Gill, D. O., et al. (2017). The weather research and forecasting model: Overview, system efforts, and future directions. *Bulletin of the American Meteorological Society*, *98*(8), 1717–1737. https://doi.org/10.1175/BAMS-D-15-00308.1

Price, C. (2009). Will a drier climate result in more lightning? *Atmospheric Research*, *91*(2–4), 479–484. https://doi.org/10.1016/j.atmosres.2008.05.016

Price, C., & Federmesser, B. (2006). Lightning-rainfall relationships in Mediterranean winter thunderstorms. *Geophysical Research Letters*, *33*, L07813. https://doi.org/10.1029/2005GL024794

Rycroft, M. J., Israelsson, S., & Price, C. (2000). The global atmospheric electric circuit, solar activity and climate change. *Journal of Atmospheric and Solar-Terrestrial Physics*, *62*(17–18), 1563–1576. https://doi.org/10.1016/S1364-6826(00)00112-7

Sátori, G., Williams, E., & Lemperger, I. (2009). Variability of global lightning activity on the ENSO time scale. *Atmospheric Research*, *91*(2–4), 500–507. https://doi.org/10.1016/j.atmosres.2008.06.014

Sátori, G., & Zieger, B. (1999). El Niňo related meridional oscillation of global lightning activity. *Geophysical Research Letters*, *26*(10), 1365–1368. https://doi.org/10.1029/1999GL900264

Skamarock, W. C., Klemp, J. B., Dudhia, J., Gill, D. O., Liu, Z., Berner, J., et al. (2019). *A description of the advanced research WRF version 4* (NCAR Technical Note NCAR/TN-556+STR). https://doi.org/10.5065/1dfh-6p97

Slyunyaev, N. N., Ilin, N. V., & Mareev, E. A. (2019). Modeling contributions of continents and oceans to the diurnal variation of the global electric circuit. *Geophysical Research Letters*, *46*, 5516–5525. https://doi.org/10.1029/2019GL083166

Slyunyaev, N. N., Ilin, N. V., Mareev, E. A., & Price, C. G. (2021a). A new link between El Niño-Southern Oscillation and atmospheric electricity. *Environmental Research Letters*, *16*(4), 044025. https://doi.org/10.1088/1748-9326/abe908

Slyunyaev, N. N., Ilin, N. V., Mareev, E. A., & Price, C. G. (2021b). The global electric circuit land-ocean response to the El Niño–Southern Oscillation. *Atmospheric Research*, *260*, 105626. https://doi.org/10.1016/j.atmosres.2021.105626

Tinsley, B. A. (2008). The global atmospheric electric circuit and its effects on cloud microphysics. *Reports on Progress in Physics*, *71*(6), 066801. https://doi.org/10.1088/0034-4885/71/6/066801

Tsonis, A. A., Elsner, J. B., Hunt, A. G., & Jagger, T. H. (2005). Unfolding the relation between global temperature and ENSO. *Geophysical Research Letters*, *32*, L09701. https://doi.org/10.1029/2005GL022875

Villafuerte, M. Q., II, & Matsumoto, J. (2015). Significant influences of global mean temperature and ENSO on extreme rainfall in Southeast Asia. *Journal of Climate*, *28*(5), 1905–1919. https://doi.org/10.1175/JCLI-D-14-00531.1

Whipple, F. J. W., & Scrase, F. J. (1936). *Point discharge in the electric field of the Earth: An analysis of continuous records obtained at Kew Observatory* (Geophys. Mem. No. 68). H. M. Stationery Off.

Williams, E., & Mareev, E. (2014). Recent progress on the global electrical circuit. *Atmospheric Research*, *135–136*, 208–227. https://doi.org/10.1016/j.atmosres.2013.05.015

Williams, E. R. (1992). The schumann resonance: A global tropical thermometer. *Science*, *256*(5060), 1184–1187. https://doi.org/10.1126/science.256.5060.1184

Williams, E. R. (2009). The global electrical circuit: A review. *Atmospheric Research*, *91*(2–4), 140–152. https://doi.org/10.1016/j.atmosres.2008.05.018

Williams, E. R., Bozóki, T., Sátori, G., Price, C., Steinbach, P., Guha, A., et al. (2021). Evolution of global lightning in the transition from cold to warm phase preceding two super El Niño events. *Journal of Geophysical Research: Atmospheres*, *126*, e2020JD033526. https://doi.org/10.1029/2020JD033526

Wilson, C. T. R. (1921). Investigations on lightning discharges and on the electric field of thunderstorms. *Philosophical Transactions of the Royal Society of London A*, *221*, 73–115. https://doi.org/10.1098/rsta.1921.0003

Wilson, C. T. R. (1924). The electric field of a thundercloud and some of its effects. *Proceedings of the Physical Society, London*, *37*, 32D–37D. https://doi.org/10.1088/1478-7814/37/1/314

Yoshida, S., Morimoto, T., Ushio, T., & Kawasaki, Z. (2007). ENSO and convective activities in Southeast Asia and western Pacific. *Geophysical Research Letters*, *34*, L21806. https://doi.org/10.1029/2007GL030758

References From the Supporting Information

Huang, B., Thorne, P. W., Banzon, V. F., Boyer, T., Chepurin, G., Lawrimore, J. H., & Zhang, H.-M. (2017a). Extended reconstructed sea surface temperature, version 5 (ERSSTv5): Upgrades, validations, and intercomparisons. *Journal of Climate*, *30*(20), 8179–8205. https://doi.org/10.1175/JCLI-D-16-0836.1

Huang, B., Thorne, P. W., Banzon, V. F., Boyer, T., Chepurin, G., Lawrimore, J. H., & Zhang, H.-M. (2017b). *NOAA Extended Reconstructed Sea Surface Temperature (ERSST), version 5*. NOAA National Centers for Environmental Information. https://doi.org/10.7289/V5T72FNM